Fused Geometric, Structural, and Control Co-Design Framework for an Energy-Harvesting Ocean Kite

Kartik Naik[1], Sumedh Beknalkar[2], Andre Mazzoleni[3], and Chris Vermillion [4]

***Abstract*— Focusing on a marine hydrokinetic energy application, this paper presents a combined geometric, structural, and control co-design framework for optimizing the performance of energy-harvesting kites subject to structural constraints. While energy-harvesting kites can offer more than an order of magnitude more power per unit of mass than traditional fixed turbines, they represent complex flying devices that demand robust, efficient flight controllers and are presented with significant structural loads that are larger with more efficient flight. While significant research has addressed the control problem, a much smaller body of research has addressed plant optimization, with no co-design effort to-date simultaneously addressing the geometry, structure, and control system. In this paper, the geometric and structural optimization is performed in what we term a nested sequential approach to minimize kite mass for a required power output, subject to structural limitations. The optimizer uses a control proxy function formulation to account for the closed-loop flight efficiency differences between different geometric designs, which accounts for plant-controller coupling without requiring explicit consideration of the controller within the geometric/structural tool itself. Medium-fidelity simulation results for a 100 kW ocean kite system illustrate the efficacy of the co-design process relative to a baseline design, and relative to a pure geometric/structural co-design that does not account for closed-loop flight efficiency through the control proxy formulation.**

I. INTRODUCTION

The tremendous potential of marine hydro-kinetic (MHK) energy for powering homes, businesses, and offshore research activities has been established in [1] and [2]. However, the deep waters associated with some of the greatest ocean current resources, along with the limited number of sites with flow resources in excess of 1 m/s (which leads to an equivalent amount of power per unit area as a 10 m/s wind resource) limits the number of sites for which towered turbines represent a viable solution for energy harvesting.

In order to unlock tidal and ocean current energy resources in locations where towered systems represent a non-viable solution, ocean kites have been studied in a large body of research over the past decade, including [3], [4], [5], and [6]. A kite-based MHK system consists of a rigid lifting body tethered to a platform, which typically flies a periodic path perpendicular to the motion of the current flow, termed a *cross-current path*. The cross-current velocities attainable by kite systems, which are dependent on the kite's lift/drag ratio, can easily be five or even ten times the flow speed [7]. Energy is generated either through an on-board rotor or through a periodic spooling operation on the tether – spooling out at high tension and spooling in at low tension to generate net positive power. Ocean kite systems represent the marine hydrokinetic analogy to the sister field of airborne wind energy systems, studied for example in [8], [9], [10], [7], [11], [12], where tethered wings are flown in crosswind patterns in order to harvest more than an order of magnitude more power per unit mass than towered systems.

The vast majority of the literature in the area of tethered wind and marine hydrokinetic energy systems, including [3], [4], [5], [6], [8], [10], [12], along with dozens of other works, focus on dynamic modeling and control aspects of these systems. Given the complexities associated with closed-loop control of crosswind/cross-current energy-harvesting motions, this level of focus is well-deserved. However, the control challenges associated with tethered systems are accompanied by a host of plant design challenges. These relate to (i) the design of an efficient kite geometry for high-speed crosswind/cross-current flight and (ii) structural design for accommodating the significant loads that are experienced during high-speed flight. These challenges are coupled with each other, as a more efficient kite geometry leads to more significant structural requirements. Furthermore, considerations of flight efficiency are coupled with control, as a designs that promise highly efficient flight based on *steady* analyses (e.g., those of [7]) have been shown not to always produce such high efficiency under actual *closed-loop operation* (as is shown, for example, in [13]). In spite of the fact that geometric and structural design have been identified as important for kite-based energy systems, along with the demonstrated fact that these attributes are coupled with the control design, the literature lacks a comprehensive effort aimed at simultaneously tackling the geometric, structural, and control attributes of energy-harvesting kite design. Focusing on an ocean kite application, this paper is the first (to the best of the authors' knowledge) to address this co-design problem.

The geometric/structural/control co-design framework in this paper is used to maximize the power-to-weight ratio of an ocean kite. The framework integrates three independent

This work was supported by the US Department of Energy under the award under the award "Device Design and Robust Periodic Motion Control of an Ocean Kite System for Hydrokinetic Energy Harvesting" [Award No. DE-EE0008635].

[1]Kartik Naik is a PhD candidate at North Carolina State University knaik@ncsu.edu.

[2]Sumedh Beknalkar is a PhD candidate at North Carolina State University sbeknal@ncsu.edu.

[3]Andre Mazzoleni is an Associate Professor in the Department of Mechanical and Aerospace Engineering at North Carolina State University, Raleigh, NC 27695, USA apmazzol@ncsu.edu.

[4]Chris Vermillion is an Associate Professor in the Department of Mechanical and Aerospace Engineering at North Carolina State University, Raleigh, NC 27695, USA cvermil@ncsu.edu. He is also a technical advisor and equity stakeholder for Altaeros Energies, Inc. and Windlift, Inc.

modules in what we refer to as a sequential-nested formulation, in order to consider bi-directional coupling between flight performance and structural performance. Specifically, an outer optimization loop makes adjustments to fuselage length and diameter. Because the optimal values of other design parameters depend on the length and diameter, *and* the optimal length and diameter depend on these other properties (which, by definition, comprises bi-directional coupling [14]), the nesting of the remainder of the optimization in an inner loop allows for convergence to an overall optimal solution [14]. An inner loop performs three sequential optimizations, which are largely unidirectionally coupled, thereby allowing for the optimizations to be performed in sequence without sacrifice to optimality. These three optimizations are performed through three tools, namely:

- A *steady flight optimization tool (SFOT)*, which selects wing and stabilizer geometric properties to minimize the kite's displaced volume (a surrogate for mass), subject to geometric and power constraints;
- A *structural wing design tool (SWDT)*, which selects spar and skin properties to minimize wing mass, subject to wing tip deflection and buoyancy considerations;
- A *structural fuselage design tool (SFDT)*, which selects the fuselage thickness to minimize fuselage mass, subject to hoop stress, sheer stress, and buckling constraints.

A closed-loop flight efficiency map, which characterizes the ratio of peak power generation to the power output predicted by steady cross-current flight calculations (as derived in [7]), is used as a *control proxy function* (CPF) within the SFOT. This CPF, which is motivated by the methodology described in [15], allows for the optimization to account for closed-loop flight inefficiencies without needing to explicitly consider the full closed-loop control system and dynamic model within the optimization framework (thus, acting as a *proxy* for the closed-loop control system).

The remainder of the paper is organized as follows. In Section II, we review the overall physical system structure and controller structure for the ocean kite under consideration. In Section III, we lay out the specifics of the co-design formulation. In Section IV, we present simulation results, showing that (i) the use of the co-design tool results in more than double the power-to-mass ratio of a baseline design first detailed in [3] and (ii) the use of the CPF within the formulation results in an additional 22 percent increase in power-to-mass ratio.

II. SYSTEM FORMULATION

The ocean kite system under consideration in this work uses a figure-8 pattern to achieve cross-current flight and generates energy at a ground station (either a platform at the ocean surface or a seabed platform) through cyclic spooling, where significant energy is generated through high-tension spool-out motions and significantly less energy is consumed through low-tension spool-in motions. Specifically, the controller uses an *intra-cycle spooling* strategy, where spooling rate is adjusted over the course of each figure-8 lap. The ground station, which houses the winch system used for spooling, is used as the inertial frame of reference for the dynamic model used in this work, as shown in Fig. 1.

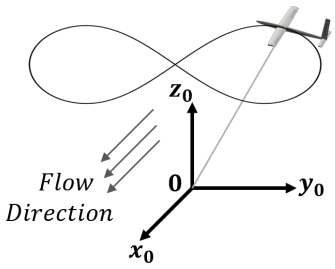

Fig. 1. The ocean kite flying in a figure-8 path, with the inertial frame of reference at the winch shown as 0 and the flow of the current being along the $\mathbf{x_0}$.

A. Plant

The kite design considered in this work is similar to that of a glider, in that it consists of the two wings, a horizontal and a vertical stabilizer, and a fuselage. Furthermore, the kite's motion is controlled through three sets of control surfaces: ailerons (which induce a rolling moment), an elevator (which induces a pitching moment), and a rudder (which predominately induces a yaw moment). The kite system has a single tether connecting it to the ground station winch.

The lift and drag characteristics for each of the kite's surfaces were parameterized using XFLR as a reference [16]. The parametric fits were obtained by running a batch analysis for several wings, where the aspect ratios were varied between 4 and 25. The net resulting hydrodynamic coefficients were fit to the following standard lift and drag curves [17]:

$$C_L = \frac{2\pi\gamma}{1+\frac{2\gamma}{e_L AR}} \cdot \alpha + C_{L,0}, \tag{1}$$

$$C_D = \left(\frac{1}{\pi e_D AR} + K_{\text{visc}}\right) \cdot (C_L - C_{L,x})^2 + C_{D,0}. \tag{2}$$

where α is the angle of attack (AoA), $C_{L,0}$ is the lift at zero AoA, γ is the airfoil lift curve multiplier, e_L is the Oswald lift efficiency, e_D is the Oswald drag efficiency, K_{visc} is the viscous drag coefficient factor, $C_{L,x}$ is the lift at minimum drag (non-zero for cambered airfoils), and $C_{D,0}$ is the drag at zero lift. The results from the batch analysis were used to tune $C_{L,0}$, γ,e_L, e_D, K_{visc}, $C_{L,x}$ and $C_{D,0}$.

A six degree of freedom (DoF) kite model, developed in [3], is used to model the dynamic behavior of the cross-current motion in a marine environment. The kite is modeled as a rigid lifting body, with forces and moments due to buoyancy, gravity and hydrodynamics. The tether dynamics are captured using a lumped mass model, each link of which is characterized as a non-compressible spring-damper as detailed in [11]. The instantaneous power generated by the power take-off system is given by:

$$P_{\text{gen}}(t) = \|\mathbf{F_{thr}}(t))\| \, v_{\text{spl}}(t) \tag{3}$$

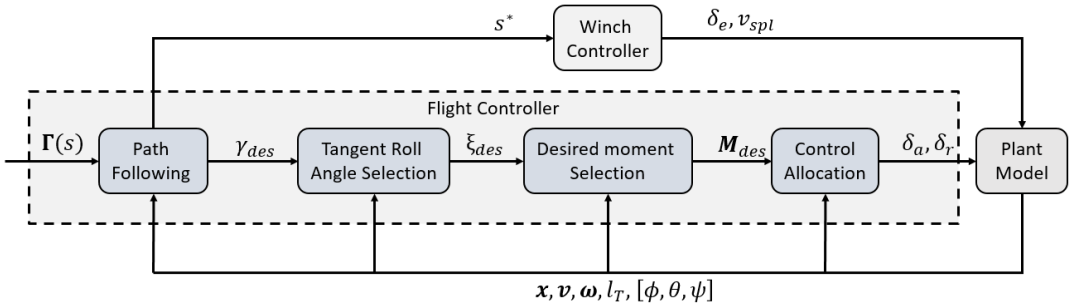

Fig. 2. Block diagram of the control system where $\boldsymbol{x}$ is the position vector, $\boldsymbol{v}$ is the velocity vector, $\boldsymbol{\omega}$ is the kite angular velocity vector, l_T is the un-spooled tether length, and $[\phi, \theta, \psi]$ is the vector of Euler angles (roll, pitch and yaw respectively.

where v_{spl} is the spooling speed and $\mathbf{F_{thr}}$ is the tether tension.

B. Controller

The objectives of the control system are two-fold:

1) Track a prescribed cross-current path (figure-8 pattern). This is controlled via commanding control surface deflections.
2) Switch between spool-in and spool-out motion in a strategic manner to ensure the flight takes place at relatively constant depth and flow speed range. This is done by adjusting the spooling speed over the course of a flight path.

This work leverages a flight controller and spooling controller designed in the co-authors' previous work [3]. The complete block diagram of the control system is shown in the Fig. 2, and the control parameters are summarized in Table I. While readers are referred to [3] for the intricate details of the control system, it is summarized here for completeness.

TABLE I
CONTROL PARAMETERS

Parameter	Description	Unit
s	path position	-
γ_{des}	desired velocity angle	rad
ξ_{des}	desired tangent roll angle	rad
$\mathbf{M_{des}}$	desired moment vector	Nm
v_{spl}	spooling speed	m/s
$[\delta_e, \delta_a, \delta_r]$	control surface deflection	rad
$\boldsymbol{x}$	position vector	m
$\boldsymbol{v}$	velocity vector	m/s
$\boldsymbol{\omega}$	angular velocity vector	rad/s
l_T	un-spooled tether length	m
$[\phi, \theta, \psi]$	Euler angles	rad

1) Flight controller: The flight controller (contained within the dashed lines of Fig. 2, takes on a hierarchical structure with four levels. The three-dimensional target cross-current path, $\Gamma(s)$, is specified based on the Lemniscate of Booth, explained in [12]. The path vector is a function of the path position s, which varies between 0 and 2π within a single figure-8 cycle and describes the kite's location on the path.

The first level of the hierarchical controller uses $\Gamma(s)$, along with the actual position of the kite, to compute a desired *velocity angle*, γ_{des}, which represents the desired direction of the kite's velocity vector. The second level maps γ_{des} to a desired tangent roll angle, ξ_{des}, which is the angle between the kite body frame y axis $\hat{y_k}$ and the so-called *tangent plane*. The tangent plane is tangent to the surface of the sphere of radius $\|\boldsymbol{x}\|$ at the kite's instantaneous position. The third level of the hierarchical controller computes a desired moment vector, $\mathbf{M_{des}}$, based on the commanded and measured tangent roll angle. Finally, at the fourth level of the hierarchical controller, the desired moments are then mapped to aileron and rudder deflections (δ_a and δ_r respectively) through a control allocation module.

2) Winch controller: The spooling motion is managed by the winch controller, which uses the kite's path position (s) to calculate the spooling speed v_{spl} and the elevator deflection δ_e to modulate the angle of the attack to generate high tension spool-out and low tension spool-out operation. Specifically, in addition to modulating the spooling speed, the controller switches δ_e from a value that yields a high angle of attack (and high lift, resulting in significant power generation) on spool-out and a value that yields a low angle of attack (and low lift, resulting in limited power consumption) on spool-in.

III. CO-DESIGN PROBLEM FORMULATION

The co-design framework seeks to solve the optimization problem that maximizes a crucial techno-economic metric, namely the kite's power-to-weight ratio (which amounts to minimizing structural mass for a required power output), while meeting performance and structural constraints. This is formulated in the following constrained optimization problem:

$$\underset{\mathbf{u}}{\text{minimize}} \quad J_p(\mathbf{u}) = \frac{P_{\text{gen}}}{m_{\text{kite}}}, \tag{4}$$

$$\text{subject to:} \quad P_{\text{req}} \leq P_{\text{gen}} \tag{5}$$

$$\mathbf{u_{min}} \leq \mathbf{u} \leq \mathbf{u_{max}} \tag{6}$$

$$C_w(\mathbf{u}) \leq 0 \tag{7}$$

$$C_f(\mathbf{u}) \leq 0 \tag{8}$$

$$m_{\text{kite}} \leq \rho_w V_{kite}. \tag{9}$$

where P_{gen} is the generated mechanical power, m_{kite} is the net structural mass of the kite, ρ_w is the density of fluid, V_{kite} is the net volume of the kite, $\mathbf{u} \in \langle s, AR, D, L, N_{\text{sp}}, t_{\text{sp}}, t_{s,w}, t_{s,f} \rangle$

includes the set of the decision variables: span (s) and aspect ratio (AR) of the wing, diameter (D) and length (L) of the fuselage, number of wing spars (N_{sp}) and their thicknesses (t_{sp}), thickness of the wing shell ($t_{s,w}$) and fuselage shell ($t_{s,f}$). Equation (5) represents a performance constraint that requires the kite to deliver the required power. Equations (7) and (8), the details of which are specified in subsequent subsections, generically describe constraint functions that capture the structural requirements of the wing and the fuselage. Finally, equation (9) represents a buoyancy constraint, which requires the displaced mass of water to exceed the required structural mass of the kite. The positively buoyant kite is ballasted with non-structural "cheap" mass to achieve the targeted neutral buoyancy for flight.

Calculating generated power as a function of design variables, as is required in equation (5), is challenging, as generated power actually depends on a combination of geometric *and* control variables. The work in [7] provides an expression for the theoretical maximum power generation of a kite executing cross-current motions, which is dependent only on properties that are derived from design parameters (specifically, the kite's lift/drag ratio and associated reference area). However, the derivation in [7] also assumes steady flight at an optimal angle of attack. In reality, the control system used to manage the kite's flight path and spooling strategy play a significant role in how close the power generation numbers match these theoretical maximums, and certain designs lend themselves to greater controllability than others. To capture the impact of closed-loop control on the kite's power generation within the design optimization framework (and the impact of the design parameters), (5) is re-written as a product of the theoretical steady flight power and a closed-loop flight efficiency factor, $\eta(\mathbf{u_p})$, where:

$$P_{\text{gen}}(\mathbf{u_p}) = \eta_f(\mathbf{u_p}) C_p(\mathbf{u_p}), \tag{10}$$

and $\mathbf{u_p}$ is the set of plant decision variables.

In (10), $\eta_f(\mathbf{u_p})$ is represents a closed-loop flight efficiency factor that behaves as a *control proxy function* (CPF). Specifically, the incorporation of $\eta_f(\mathbf{u_p})$ within the optimization framework allows for the consideration of the closed-loop efficiency afforded by the controller without requiring the optimization framework to account for the full dynamic model and control system. The efficiency map, $\eta_f(\mathbf{u_p})$, was generated by performing a parametric sensitivity study to capture the impact of key geometric parameters, namely the kite's aspect ratio and span (AR and s), which were determined to be most influential to closed-loop flight efficiency. This is further explained in detail in Section III-E.

While the utility of the CPF is similar to the one described in [15], it is used in a multiplicative manner rather than additive. The formulation of the constraint in (5) and the process of mapping it in the design space is shown in Sections III-A and III-E respectively.

Fig. 3 shows the methodology used to formulate the co-design problem, which is solved via what we term a *nested-sequential* approach. Specifically, an outer loop iterates on

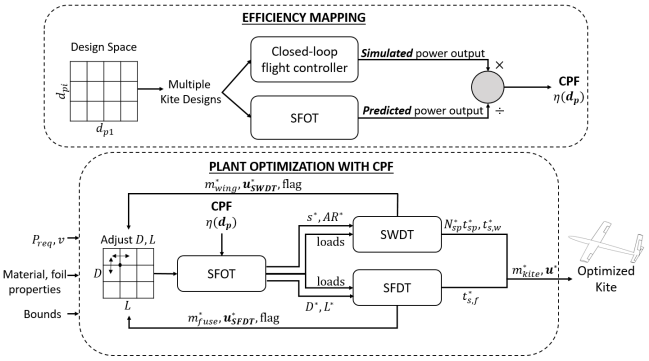

Fig. 3. Co-Design framework: Kite designs are simulated in the to obtain a CPF. The CPF is then used in the nested co-design formulation to arrive at a system optimum.

the fuselage diameter (D) and length (L). An inner optimization loop, which addresses the remaining design variables, is partitioned into three modules that are executed in sequence: the *steady flight optimization tool (SFOT)*, the *structural wing design tool (SWDT)*, and the *structural fuselage design tool (SFDT)*. Each module solves an optimization subproblem in a nested framework to account for the *coupling* between the modules. The nested formulation (specifically, the consideration of D and L within an outer loop) arises due to bi-directional coupling introduced through the partitioning of the SFOT, SWDT, and SFDT. In particular, the required fuselage diameter and length are dependent on structural considerations, but these are dictated by the wing loads, which are in turn dependent on the optimization of flight performance. Given this coupling, a sequential approach to selecting D and L will, in general, not lead to an optimal design. Thus, D and L are adjusted within an outer loop, whereas the other unidirectionally coupled variables (for which the choice of span (s) and aspect ratio (AR) significantly influence optimal values of structural design variables, but not vice versa) are considered in sequence, within an inner loop.

A. Steady flight optimization tool

The steady flight optimization tool seeks to obtain the most compact wing design that can produce the required power for a rated flow speed. This is done is by minimizing the wing volume while meeting the performance and geometric constraints:

$$\underset{\mathbf{u}}{\text{minimize}} \quad V_{\text{wing}}(\mathbf{u}) = K\frac{s^3}{AR^2}, \tag{11}$$

$$\text{subject to:} \quad \max_{\mathbf{u}}\left(\frac{2}{27}\right)\frac{\eta_f \rho_w v^3 s^2}{AR^2}\left(\max_{\alpha}\frac{C_L^3}{C_D^2}\right) \geq P_{\text{req}} \tag{12}$$

$$\mathbf{u_{min}} \leq \mathbf{u} \leq \mathbf{u_{max}}. \tag{13}$$

where $\mathbf{u} \in \langle s, AR \rangle$ are the decision variables, η_f is the flight efficiency (explained in section III-E), v is the rated flow speed, C_L and C_D are the lift and drag coefficients of the whole kite, and α is the angle of attack. The generated

mechanical power estimate shown in (12) was derived in [7].

B. Structural wing design tool

The lifting loads acting on the wing produce a large bending moment about the chord-wise neutral axis. The wing structural design tool minimizes the structural support mass required to support the wing. The structure is designed as a combination of spars and shell. The SWDT solves the mixed-integer constrained optimization problem formulated as:

$$\underset{\mathbf{u}}{\text{minimize}} \quad m_{\text{wing}}(\mathbf{u}) = \rho_m s A_{\text{wing}}(\mathbf{u}), \tag{14}$$

$$\text{subject to:} \quad I_{\text{wing}} = I_{\text{req}} \mid \delta_{\max} \tag{15}$$

$$\mathbf{u_{min}} \leq \mathbf{u} \leq \mathbf{u_{max}}. \tag{16}$$

where ρ_m is the material density, A_{wing} is the total cross-sectional area, and $\mathbf{u} \in \langle N_{\text{sp}}, t_{\text{sp}}, t_{s,w} \rangle$ are the decision variables. The bounds on the decision variables are as follows:

- N_{sp} is an integer type decision variable and can take integer values among $N_{\text{sp}} \in (1,2,3)$;
- Bounds on both t_{sp} and $t_{\text{s,w}}$ are linear functions of the chord length c of the wing, given by: $t_{\text{sp,min}}(c) \leq t_{\text{sp}} \leq t_{\text{sp,min}}(c)$, $t_{\text{s,w,min}}(c) \leq t_{\text{s,w}} \leq t_{\text{s,w,min}}(c)$.

Equation (15) formulates the required moment of inertia of the wing-spar as equality constraint, where I_{req} is calculated for a maximum wing tip deflection $\delta_{\max}$ due to lift. The moments of the inertia calculated for the spars and the shell are estimated as the sum of discretized rectangular beams with varying heights to retain the shape of the hydrofoil. A representative cross-sectional design of the wing structure is shown in Fig. 4.

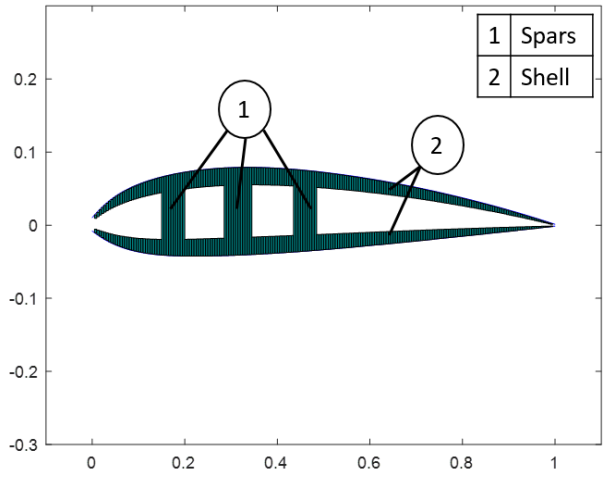

Fig. 4. Sample output of SWDT: Cross-section of a wing with N_{sp}=3 , t_{sp} = 0.068 m and t_{sp} = 0.039 m.

C. Structural fuselage design tool

The structural fuselage design tool minimizes the mass of the fuselage while meeting several structural constraints. A simplifying assumption is made to design the fuselage as a cylindrical shell. The SFDT solves the optimization problem formulated as:

$$\underset{\mathbf{u}}{\text{minimize}} \quad m_{\text{fuse}}(\mathbf{u}) = \rho_m A_{\text{fuse}}(\mathbf{u}) L, \tag{17}$$

$$\text{subject to:} \quad \frac{\sum F_z}{t_{s,f} L} \leq \zeta \sigma_{\text{yield}} \tag{18}$$

$$\frac{PD}{2t_{s,f}} \leq \zeta \sigma_{0.5} \tag{19}$$

$$\frac{|M_{\max}|}{S(\mathbf{u})} \leq \zeta \sigma_{\text{yield}} \tag{20}$$

$$\mathbf{u_{min}} \leq \mathbf{u} \leq \mathbf{u_{max}} \tag{21}$$

where A_{fuse} is the cross-sectional area of the fuselage, and $\mathbf{u} \in \langle D, L, t_{s,f} \rangle$ are the decision variables. The structural constraint equations are explained as follows [18]:

- *Shear stress:* Equation (18) models the shear behaviour due tangential loads wing and stabilizer attachment points. F_z are the loads in the direction normal to the wing, ζ is the factor of safety, and the σ_{yield} is the yield stress of the material.
- *Hoop stress:* The fuselage of the kite is assumed to be a thin-walled pressure vessel. The difference in the external and internal pressures, P, causes circumferential stresses due to increased static and dynamic pressure during cross-current flight. $\sigma_{0.5}$ is the stress at 0.5 % elongation.
- *Buckling:* The lift forces of the wings and the horizontal stabilizer induce buckling loads about the tether attachment point. $|M_{\max}|$ is the maximum buckling moment calculated for set of hydrodynamic forces, and $S(\mathbf{u})$ is the section modulus of the fuselage.

D. Coupling

1) SFOT-SWDT: The kite generates more power with large spans (s) and high aspect ratios (AR), which result in small chord lengths. This conflicts with SWDT, which tends to minimize the span and aspect ratio of the wing for a rigid structural support. Thus, for a given load profile generated by the SFOT, the SWDT requires a minimum chord length for a structurally feasible design.

2) SFOT-SFDT: The total drag of the kite is heavily influenced by the diameter of the fuselage. While the SFOT tries to minimize the fuselage diameter, a minimum diameter is required by the SFDT to design for the structural loads on the fuselage.

E. Closed-loop flight efficiency map

The three aforementioned modules, namely SFOT, SWDT, and SFDT, collectively comprise a plant optimization. The value of P_{gen} estimated in (12) is based on steady cross-current flight performance of the kite. This is an idealized estimate that does not account for transient effects associated with the kite's acceleration and deceleration within a figure-8 cycle. Furthermore, the idealized estimate in (12) assumes that the kite can be spooled in infinitely fast, under zero tension.

The closeness of the kite's actual power output to steady cross-current flight predictions depends significantly on the kite's closed-loop control performance. For the ocean kite system, the controller has a largely unidirectional coupling with the plant, wherein the plant decision variables $\mathbf{u_p}$ significantly impact the optimal achievable control performance, but knowledge of the controller is significantly less important in optimizing the plant. This dependence was studied through a sensitivity analysis, whereby the influence of key plant parameters within $\mathbf{u_p}$ on flight efficiency was characterized. Thus, a flight efficiency term can be defined as:

$$\eta_f = \frac{P_{\text{gen}}}{P_{\text{ideal}}} \tag{22}$$

where P_{gen} is the peak mechanical power observed in one cycle during simulation with the closed-loop flight controller, and P_{ideal} is the theoretical steady state power calculated in (12) with $\eta_f = 1$.

As the parameters optimized in the SFOT, namely $\mathbf{u_p} \in \langle s, AR \rangle$, dictate the flight, these parameters were chosen for the sensitivity analysis that was used to generate the closed-loop efficiency map. Multiple kites with s varying from 8 to 10 m, and AR varying from 6 to 14 were simulated to map a surface of η_f. A least squares fit of the surface was then used to obtain $\eta_f(s, AR)$, which was used as a multiplicative control proxy function (CPF) as formulated in (10). The efficiency map resulting from the sensitivity analysis is shown in Fig. 5.

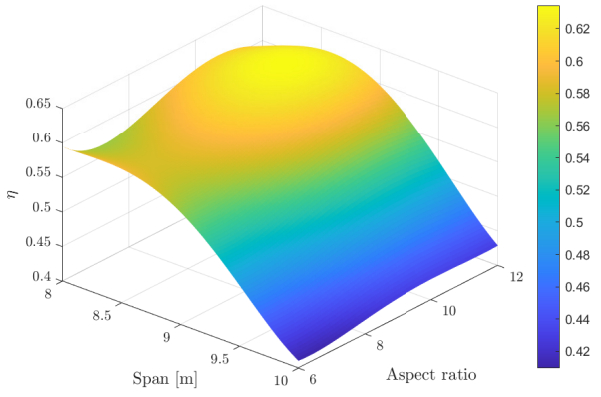

Fig. 5. Results of sensitivity analysis: A flight efficiency map that relates the dynamically simulated power generated P_{gen} to the theoretically calculated and optimized power P_{ideal} calculated in (12).

IV. RESULTS

TABLE II
SIMULATION PARAMETERS

Property	Description	Value	Unit
δ_{max}	Max. wingtip deflection (% of span)	5	-
σ_{yield}	yield strength of material	2.70E+08	*Pa*
E	young's modulus of material	6.89E+10	*Pa*
P	pressure difference	2.50E+03	*Pa*
γ	lift curve multiplier	9.60E-01	-
e_L	oswald lift efficiency	7.60E-01	-
e_D	oswald drag efficiency	9.20E-01	-
$C_{L,0}$	zero AoA lift coefficient	1.60E-01	-
$C_{L,x}$	lift at minimum drag	2.00E-02	-
K_{visc}	viscous drag factor	3.00E-02	-
$C_{D,0}$	drag at zero lift	6.50E-03	-
ρ_w	density of water	1.00E+03	kg/m^3
ρ_m	density of **(wing)** material	2.70E+03	kg/m^3

The co-design framework was used to solve the optimization problem discussed in Section III. The kite's performance, characterized by the power-to-weight ratio, was compared for three designs:

1) *Baseline design*: The kite design used in the co-author's previous work [3], which uses a span of 10 m and an aspect ratio of 11.1, was used for the baseline. This previous work focused heavily on the design of the hierarchical kite control system but minimally on the coupling of the plant design with this control system design.
2) *Co-design without efficiency map (CPF)*: This kite design is the product of using the design optimization tool with the flight efficiency factor, η_f, modeled as constant (i.e., no coupling between closed-loop flight efficiency and plant parameters was considered here). For this work, the efficiency of the baseline design was used as the fixed value of η_f.
3) *Co-design optimized kite using the efficiency mapping*: Here, the proposed co-design tool, with the closed-loop flight efficiency map arising from the aforementioned sensitivity analysis, was used for the co-design process.

Table II lists the fixed parameters and constraint values used for the co-design process. The hydrodynamic surfaces each use a NACA 2412 foil, and Al 6061 as the primary structural material. Fig. 6 compares the simulated performance of the aforementioned kites. Though the kite mass is constant and only the generated power varies with time, power-to-weight ratio (or specific power) is a more apt metric to compare performance. This is because all designs (by the nature of the optimization formulation, where power output serves as a constraint) produce nearly the same power output, but with dramatically different masses. Moreover, this work focuses on the techno-economic metric where the objective of the overall optimization problem is to maximize the power-to-weight ratio.

Table III provides a summary of the baseline design and the optimized designs obtained through the proposed co-design formulation with and without the closed-loop flight efficiency map acting as the CPF. Here, F_{max} is the

TABLE III

RESULTS: COMPARISON OF OPTIMIZED KITE DESIGNS.

Property	**Baseline**		**Without CPF**		**With CPF**		**Unit**
AR	**11**		**7.9**		**7.4**		–
s	**10.00**		**8.82**		**8.54**		m
D	0.65	–	0.5		0.5		m
L	7.5	–	6.5	7.1	6.5	7	m
v	1.5	2	1.5	2	1.5	2	m/s
F_{max}	362	583	261	541	250	528	kN
I_{req}	293.7	473.3	164.3	328.6	147.4	306.6	in^4
N_{sp}	2	–	1	2	1	2	–
t_{sp}	0.2100	–	0.0054	0.0090	0.0050	0.0060	m
$t_{s,w}$	0.14	–	0.15	0.18	0.1	0.15	m
m_{wing}	**2321**	**–**	**704**	**1521**	**536**	**1260**	kg
$t_{s,f}$	0.03	–	0.01	0.01	0.01	0.01	m
m_{fuse}	413.5	–	275.7	301.2	275.7	296.8	kg
m_{kite}	**2734**	**–**	**989.7**	**1822.2**	**811.7**	**1554.8**	kg
P_{avg}	**34.5**	**98.9**	**34.5**	**94.1**	**34.8**	**94.6**	kW
$P_{\text{avg}}/m_{\text{kite}}$	**0.012**	**–**	**0.035**	**0.055**	**0.043**	**0.064**	kW/kg
$P_{\text{peak}}/m_{\text{kite}}$	**0.062**	**–**	**0.131**	**0.141**	**0.156**	**0.172**	kW/kg

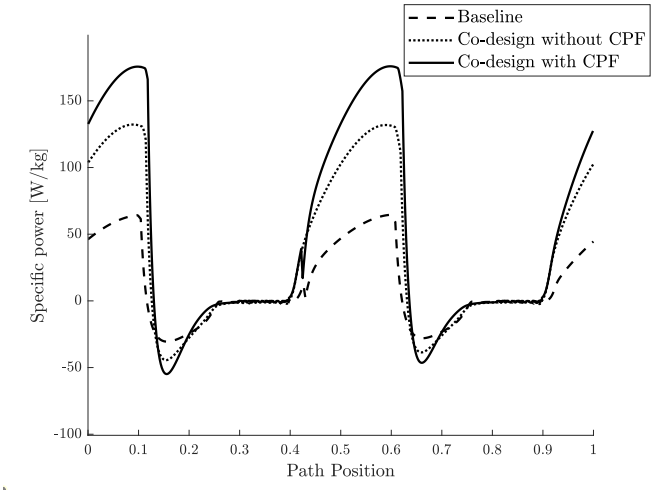

Fig. 6. Results comparing the specific power of the baseline with the co-design optimized kite with and without the CPF. The optimized kites outperform the baseline, while the kite using the CPF performs moderately better than with an arbitrary efficiency estimate. The results show the kites' flight performance over a single lap in a constant flow regime, with flow speed of 1.5 m/s.

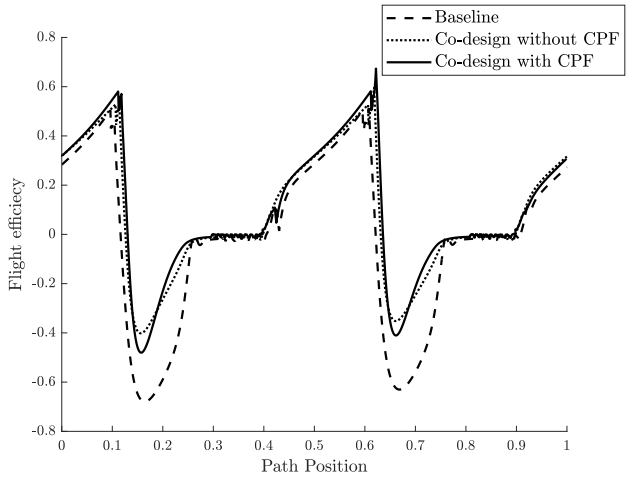

Fig. 7. Results comparing the flight efficiency η of the baseline, optimized kites - with and without the CPF. The results show the kites' flight efficiencies over a single lap in a constant flow regime, with flow speed of 1.5 m/s.

maximum total force that acts in a direction normal to the wing and causes bending. Note that two sets of analyses were performed, simulated at flow speeds of 1.5 and 2 m/s, resulting in *two sets* of kite designs. Results in Fig. 6 and Fig. 7 respectively show the comparison of flight efficiencies and power-to-weight ratios, simulated at 1.5 m/s flow speed.

The optimized designs generate comparable lap-averaged powers but accomplish this with significantly less mass, making them much more techno-economically efficient. The observed reduction in total mass - mainly arising from a reduction in wing structural mass - is due to much higher requirements of area moments of inertia for larger spans. Note that, as flow speeds increase, F_{max} significantly increases. This results is higher tether tensions and consequently higher power generation, but also amplifies the structural design challenge of packing a support structure that can bear the structural loads while restricting the wing tip deflections to δ_{max}. Thus, for the chosen material (Al 6061), no feasible structural design was found for the baseline kite in these cases.

V. CONCLUSIONS AND FUTURE WORK

In this work, we presented a combined geometric, structural, and control co-design formulation for an ocean kite that resulted in significantly increased power-to-mass ratios relative to a baseline design. The formulation relies on a closed-loop flight efficiency map, which serves as a control proxy function (CPF), to capture the coupling between the plant

and control design while not requiring explicit consideration of the controller within the geometric-structural optimization tool. Future work will focus on the extension of the proposed tool to account for site-specific flow characteristics (as described through flow histograms) and levelized cost of energy (requiring a modeling framework that estimates capital and operational costs as functions of design parameters).

ACKNOWLEDGMENT

The authors would like to thank Dr. Hosam K. Fathy for his guidance and useful suggestions. The authors would also like to thank lab members Dr. Mitchell Cobb, James Reed, Ayaz Siddqui and John Borek for their support and legacy work in the closed-loop controller design.

REFERENCES

[1] K. Haas, "Assessment of energy production potential from ocean currents along the united states coastline," Georgia Tech Research Corporation, Tech. Rep., 2013.

[2] A. LiVecchi, A. Copping, D. Jenne, A. Gorton, R. Preus, G. Gill, R. Robichaud, R. Green, S. Geerlofs, S. Gore, *et al.*, "Powering the blue economy; exploring opportunities for marine renewable energy in maritime markets," *US Department of Energy, Office of Energy Efficiency and Renewable Energy. Washington, DC*, p. 207, 2019.

[3] J. Reed, J. Daniels, A. Siddiqui, M. Cobb, and C. Vermillion, "Optimal exploration and charging for an autonomous underwater vehicle with energy-harvesting kite," in *2020 American Control Conference (ACC)*. IEEE, 2020, pp. 4134–4139.

[4] A. Ghasemi, D. J. Olinger, and G. Tryggvason, "Computational simulation of the tethered undersea kites for power generation," in *ASME International Mechanical Engineering Congress and Exposition*, vol. 57441. American Society of Mechanical Engineers, 2015.

[5] H. Li, D. J. Olinger, and M. A. Demetriou, "Control of a tethered undersea kite energy system using a six degree of freedom model," in *2015 54th IEEE conference on decision and control (CDC)*. IEEE, 2015, pp. 688–693.

[6] A. Siddiqui, K. Naik, M. Cobb, K. Granlund, and C. Vermillion, "Lab-scale, closed-loop experimental characterization, model refinement, and validation of a hydrokinetic energy-harvesting ocean kite," *Journal of Dynamic Systems, Measurement, and Control*, vol. 142, no. 11, 2020.

[7] M. L. Loyd, "Crosswind kite power (for large-scale wind power production)," *Journal of energy*, vol. 4, no. 3, pp. 106–111, 1980.

[8] P. Williams, B. Lansdorp, and W. Ockesl, "Optimal crosswind towing and power generation with tethered kites," *Journal of guidance, control, and dynamics*, vol. 31, no. 1, pp. 81–93, 2008.

[9] R. Schmehl, *Airborne Wind Energy*. Springer, 2018.

[10] "Airborne wind energy: An overview," in *American Control Conference*, 2012.

[11] C. Vermillion, T. Grunnagle, R. Lim, and I. Kolmanovsky, "Model-based plant design and hierarchical control of a prototype lighter-than-air wind energy system, with experimental flight test results," *IEEE Transactions on Control Systems Technology*, vol. 22, no. 2, pp. 531–542, 2013.

[12] S. Rapp, R. Schmehl, E. Oland, S. Smidt, T. Haas, and J. Meyers, "A modular control architecture for airborne wind energy systems," in *AIAA Scitech 2019 Forum*, 2019, p. 1419.

[13] P. Nikpoorparizi, N. Deodhar, and C. Vermillion, "Modeling, control design, and combined plant/controller optimization for an energy-harvesting tethered wing," *IEEE Transactions on Control Systems Technology*, vol. 26, no. 4, pp. 1157–1169, 2017.

[14] H. K. Fathy, J. A. Reyer, P. Y. Papalambros, and A. Ulsov, "On the coupling between the plant and controller optimization problems," in *Proceedings of the 2001 American Control Conference.(Cat. No. 01CH37148)*, vol. 3. IEEE, 2001, pp. 1864–1869.

[15] D. L. Peters, P. Papalambros, and A. Ulsoy, "Control proxy functions for sequential design and control optimization," *Journal of Mechanical Design*, vol. 133, no. 9, 2011.

[16] M. Drela, H. Youngren, M. Scherrer, and A. Deperrois, "Xflr-5," 2012.

[17] E. Torenbeek, *Synthesis of subsonic airplane design: an introduction to the preliminary design of subsonic general aviation and transport aircraft, with emphasis on layout, aerodynamic design, propulsion and performance*. Springer Science & Business Media, 2013.

[18] D. Roylance, "Pressure vessels," *Department of Materials Science and Engineering, Massachusetts Institute of Technology, Cambridge*, 2001.